

Manifestations of the hyperfine interaction between electron and nuclear spins in singly-charged (In,Ga)As/GaAs quantum dots

Roman V. Cherbunin and Ivan V. Ignatiev*

*Experimentelle Physik II, Technische Universität Dortmund, 44221 Dortmund, Germany and
Institute of Physics, St. Petersburg State University, St. Petersburg, 198504, Russia*

Thomas Auer, Alex Greulich, Ruth Oulton[†], and Manfred Bayer

Experimentelle Physik II, Technische Universität Dortmund, 44221 Dortmund, Germany

Dmitri R. Yakovlev

*Experimentelle Physik II, Technische Universität Dortmund, 44221 Dortmund, Germany and
Ioffe Physico-Technical Institute, 194021 St. Petersburg, Russia*

Gleb G. Kozlov

Institute of Physics, St. Petersburg State University, St. Petersburg, 198504, Russia

Dirk Reuter and Andreas D. Wieck

Angewandte Festkörperphysik, Ruhr-Universität Bochum, D-44780 Bochum, Germany

(Dated: November 15, 2018)

The nuclear spin fluctuations (NSF) as well as the dynamic nuclear polarization (DNP) and their effects on the electron spins in negatively charged (In,Ga)As/GaAs quantum dots have been studied by polarized pump-probe and photoluminescence spectroscopy techniques. The effective magnetic field of the NSF is about 30 mT at low excitation power. The NSF distribution becomes highly anisotropic at strong optical excitation by circularly polarized light with periodically alternating helicity. This phenomenon is attributed to a decrease of the nuclear spin entropy due to the hyperfine interaction with polarized electron spins. The DNP is limited to small values for intense, but short photoexcitation.

PACS numbers: 72.25.Fe, 78.67.Hc, 71.70.Jp

I. INTRODUCTION

The strong localization of the electron wave function in a quantum dot (QD) leads to a considerable increase of the electron density at the nuclear sites and, therefore, enhances the hyperfine interaction of the electron spin with the nuclear spins^{1,2,3}. The interaction changes the electron and nuclear spin dynamics, and can be described by a Fermi contact-type Hamiltonian which couples the electron spin \mathbf{S} and a nuclear spin \mathbf{I}_i :

$$\hat{H} = \sum_i A_i |\psi(\mathbf{R}_i)|^2 \left(\hat{S}_z \hat{I}_{i,z} + \hat{S}_+ \hat{I}_{i,-} + \hat{S}_- \hat{I}_{i,+} \right), \quad (1)$$

where the sum goes over all nuclei in the QD electron localization volume. The interaction strength of the electron with the i -th nucleus is determined by the hyperfine constant A_i and the electron density $|\psi(\mathbf{R}_i)|^2$ at the nuclear site \mathbf{R}_i . \hat{H} mediates processes in which the spins of electron and nucleus are mutually flipped, as described by the products of raising and lowering operators \hat{S}_\pm and $\hat{I}_{i,\pm}$, which increase and decrease the spin projections S_z and $I_{i,z}$ along the quantization axis z , respectively. Two effects of the hyperfine interaction on polarized electron spins are possible.

First, due to the limited number of nuclear spins interacting with the electron spin in the QD, typically on the

order of $N_L \sim 10^5$, a random correlation of the nuclear spins may create a small nuclear polarization fluctuating from dot to dot. The nuclear spin fluctuations (NSF) act on the electron spins as an effective magnetic field, $B_f \propto 1/\sqrt{N_L}$, with random magnitude and orientation⁴. The electron spin precession about this field gives rise to a relatively fast dephasing of the electron spins in a QD ensemble and, therefore, to a decay of the electron spin polarization. Theoretical estimates for GaAs QDs give dephasing times in the nanoseconds range^{4,5} and predict a three-fold decrease of the electron spin polarization in an ensemble due to the precession. Experiments performed so far confirm a rapid electron spin dephasing in an InAs QD ensemble due to the spin precession in the NSF field^{7,8}. Thereafter, due to relatively slow flip-flop processes in the nuclear spin system which change the NSF orientation on a microsecond time scale, the electron spin orientation may be further destroyed. This is assumed to be the most efficient relaxation mechanism for electron spins in QDs^{4,5} due to the suppression of other mechanisms, in particular of the electron spin relaxation via the spin-orbit interaction⁶. For completeness we note that the hyperfine interaction is found to be also the main relaxation mechanism of electron spins at cryogenic temperatures in n-doped bulk GaAs⁹ and GaAs/(Al,Ga)As quantum wells^{10,11}.

The second effect of the hyperfine interaction appears

when the nuclear spins have been polarized somehow. The hyperfine interaction with polarized nuclear spins affects the electron spin like an effective magnetic field (the nuclear field), B_N , causing a Zeeman splitting of electronic levels or an energy shift of them (the Overhauser shift) in presence of an external magnetic field. This effect has been observed in single-dot spectroscopy studies^{3,12,13,14,15,16,17,18,19,20}. In particular, an Overhauser shift of several tens of μeV for GaAs interface QDs has been found³ which corresponds to a 65% polarization of the nuclear spins and a nuclear field $B_N \sim 1.2$ T.

A nuclear spin polarization considerably affects also the electron spin relaxation. First, when the electron spin is oriented parallel to the nuclear field, the NSF effect is weakened because the electron spin precesses about the total field whose orientation is close to that of B_N when $B_N \gg B_f$. Second, the polarization of nuclear spins damps their flip-flop processes²¹ and, correspondingly, suppresses electron spin relaxation related to the NSF re-orientation. Recent experiments have demonstrated very long spin memories in QDs^{22,23,24,25,26,27} even though the role of the nuclear spin polarization in this effect is still not totally clarified yet.

The nuclear spin dynamics may be also considerably modified by the hyperfine interaction with polarized electron spins. The creation of a dynamic nuclear polarization (DNP) via interaction with optically polarized electrons is well known and has been extensively discussed in literature (see, e.g., Ref. 28).

The DNP magnitude is usually measured by detecting the Overhauser shift of optical transitions from (or to) electron Zeeman levels. Due to the required high spectral resolution such measurements are possible only on single QDs because of the large inhomogeneous broadening of the optical transitions in a dot ensemble (typically larger than 10 meV) compared to the Overhauser shift (a few or several tens of μeV). Another method relies on studying the photoluminescence polarization in a longitudinal or tilted magnetic field, and has been successfully exploited for bulk semiconductors (see in Ref. [28] Chs. 2 and 5). However, it has still not been applied widely to QDs²⁹. To date, little is known about the DNP magnitude in a QD ensemble and the role of DNP in the electron spin relaxation²⁶. The NSF effect has also hardly been studied because of the lack of sensitive experimental methods⁷. In particular, nothing is known about the effect of the electron spin polarization on the NSF.

Here we present results of detailed investigations of the hyperfine interaction in singly negatively charged (In,Ga)As/GaAs self-assembled QDs. Due to the presence of the resident electron in a QD, its spin is an efficient tool for probing the nuclear spin system. Exploiting two experimental methods, we have studied the effects of NSF and DNP on the spin polarization of the resident electrons in the QDs. In particular, we have obtained the average magnitudes of the effective magnetic fields of NSF and DNP and their dependence on the polarization and power density of the optical excitation.

Recently we have studied the electron-nuclei interaction in a regime in which we observed indications for a strong coupling between the two systems, leading to the formation of a “nuclear spin polaron” complex²⁶. These indications were found under conditions of strong optical pumping realized by both high optical excitation powers and long illumination times. Here we address another regime, in which only rather short optical exposure times were used. The goal of our study was to develop an understanding of nuclear effects under these conditions, which would correspond to the initial stages of nuclear polaron formation.

II. EXPERIMENT

We studied two samples containing 20 layers of (In,Ga)As/GaAs self-assembled QDs separated by 60 nm thick GaAs barriers. Si- δ doped layers are incorporated 20 nm below each dot layer. The as-grown InAs QD sample underwent a post-growth rapid thermal annealing treatment for a duration of 30 s, either at a temperature of 900°C (sample #1) or 945°C (sample #2). This leads to diffusion of indium out of the QDs³⁰, and results in a shift of the photoluminescence (PL) photon energy of the QD ground state from ~ 1.03 eV for the as-grown sample to 1.338 and 1.396 eV for the annealed samples, respectively. The average carrier concentration in the QDs due to the barrier delta-doping is approximately one electron per dot, as confirmed by Faraday rotation spectroscopy³¹. We studied also a quantum well heterostructure with two coupled 8 nm wide In_{0.09}Ga_{0.91}As quantum wells separated by a thin, 1.7 nm wide GaAs barrier was grown as a reference sample on an undoped GaAs substrate by molecular beam epitaxy. It contains an n-doped GaAs buffer layer which serves as source of electrons for the QWs. The two-dimensional electron gas density in the QWs does not exceed 10^{10} cm⁻². The samples were immersed in pumped liquid helium at temperature $T = 2$ K.

We have explored the dynamics of the electron spin polarization induced by circularly polarized pump pulses from a Ti:Sapphire laser (pulse duration 1.5 ps at a pulse repetition frequency 75.6 MHz). Excitation with a fixed polarization helicity (either σ^+ or σ^-) was used to study the DNP effect. When we studied the NSF effect, the DNP was suppressed by modulation of the circular polarization between σ^+ and σ^- (hereafter referred to as σ^+/σ^- -excitation) at a frequency of 25 or 50 kHz. A photo-elastic modulator or an electro-optical modulator with sharp leading and falling edges (< 1 μs) of the pulses followed by a quarter wave plate was used for polarization control.

Two types of experiments were performed. First, we used resonant optical excitation of the lowest optical QD transition and measured the Faraday rotation signal (see details in Sec. III). Second, we measured the circular polarization of the PL, both time-integrated and

time-resolved, under non-resonant excitation of the QDs. Time-resolved PL spectra were detected by a synchro-scan streak camera attached to an 0.5-m spectrometer. The time resolution was about 20 ps.

In the time-integrated measurements of the PL, we used special timing protocols for modulation of the excitation intensity and polarization. The intensity was modulated by an acousto-optical modulator, which formed microsecond-long trains of picosecond pulses. Four trains each of $7.5 \mu\text{s}$ duration with varying polarizations formed a series which was repeated each $40 \mu\text{s}$. The primal polarization of the laser beam was σ^+ . When we studied the NSF effect, the polarization of the two last pulses within a period was changed by an electro-optical modulator from σ^+ to σ^- so that the excitation was non-polarized on average. This was done to avoid DNP in the QDs. In the study of the DNP effect, the polarization was modulated non-symmetrically, i.e., three pulses had one helicity and the fourth one had opposite helicity, to obtain non-zero time-averaged circular polarization of the excitation. The PL was detected for σ^+ polarization during the second and fourth pulses which were σ^+ - and σ^- -polarized in both cases, respectively. The timing protocols therefore allowed us to study both nuclear spin effects under almost identical experimental conditions. Note that subsequent pulses in each train are separated by a 13.2-ns time interval which is too short to change the electron or the nuclear spin dynamics. Therefore a pulse train should have the same impact as a pulse of the same duration as the train, and we will denote in the following a pulse train just as long pulse.

All experiments were performed in a longitudinal magnetic field oriented parallel to the structure growth axis and the light wavevector (Faraday geometry). The field defines the spin quantization axis, which we take as the z -axis [see Eq. (1)]. In this geometry, the components $B_{N,x}$ and $B_{N,y}$ of the nuclear field normal to the external field are determined by the NSF, while the component $B_{N,z}$ is determined by both the NSF and DNP.

III. NSF EFFECT IN FARADAY ROTATION

Faraday rotation (FR) spectroscopy has been widely exploited for studying spin dynamics (see, e.g., Ref. [32], Ch. 5). Using this technique, sketched in Fig. 1(b), the circularly polarized pump beam orients the electron spins along the optical axis and the linearly polarized probe beam tests it. Detected is the rotation angle of the probe polarization plane. The rotation occurs due to the photo-induced Faraday effect which arises from an effective magnetization created by the optically oriented electron spins in the QDs leading to circular birefringence of the sample. We used a degenerate pump-probe method in which the wavelengths of pump and probe are the same.

We have studied the FR signal of the QD samples in dependence of the longitudinal magnetic field. Typical

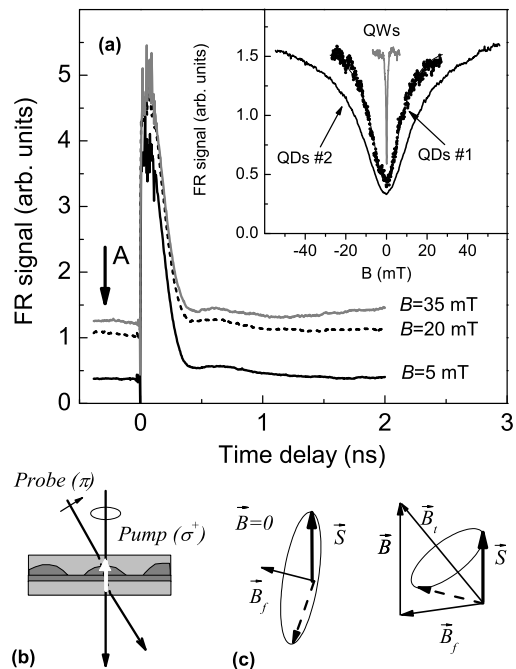


FIG. 1: (a) FR signal of sample #2 for different longitudinal magnetic field strengths, as noted at each curve. Sample temperature $T = 2 \text{ K}$; pump power density $P = 20 \text{ W/cm}^2$. The arrow A shows the time delay at which the magnetic field dependence of the signal amplitude was measured. Inset: field dependence of the FR signal for different studied samples. (b) Schematic illustration of the polarization resolved pump-probe method for measuring Faraday rotation (see text). (c) Mechanism of suppression of the NSF effect by an external magnetic field.

traces of the signal versus the delay between pump and probe are shown in Fig. 1(a). They were measured for σ^+ / σ^- -excitation for which no DNP occurs. Each trace consists of a rapidly decaying and a long-lived component. The fast component with a decay time of about 0.3 ns is related to recombination of the electron-hole pairs created by the strong pump pulse. The long-lived component is due to spin polarization of the resident electrons^{31,33}.

Application of a relatively small magnetic field causes a strong increase of the amplitude of the long-lived FR component so that it becomes pronounced even at negative delays where it originates from the preceding laser pulses. We measured the field dependence of the FR signal at a fixed negative delay time indicated by the arrow. This delay is ~ 13 -nanoseconds after the preceding pulse, at which all processes such as electron-hole recombination, have decayed and the signal is determined solely by the spin orientation of the resident electrons. The inset in Fig. 1(a) shows the magnetic field dependence of the FR signal which reveals a dip around $B = 0$. Its full width at half maximum (FWHM) varies considerably for

the different studied samples.

The dip in the field dependence can be explained by the model of Merkulov *et al.*⁴ which is illustrated in Fig. 1(c). The electron spin \vec{S} is initially oriented by laser excitation along the optical excitation axis which coincides with the growth direction of the heterostructure. In presence of the NSF and an external magnetic field B , the electron spin rapidly precesses about the total field, $\mathbf{B}_t = \mathbf{B}_f + \mathbf{B}$ with a frequency $\omega = |g_e|\mu_B B_t/\hbar$ where $|g_e| \approx 0.5$ is the QD electron g -factor and μ_B is the Bohr magneton. This precession results in an oscillation of the spin projection onto the z -axis for each QD. Because of the spread of B_f in the dot ensemble, the oscillations in different dots occur with different frequencies. Destructive interference of the oscillations gives rise to a decay of the z -projection of the average electron spin in the ensemble. The FR signal is proportional to this z -projection of the spin and, therefore, is expected to decay too. For zero external magnetic field, the decay time may be estimated using a Gaussian distribution for B_f [see Ref. 4]: $\tau_{NSF} = 1/\omega \sim 1$ ns, where we used a value $B_f = 15$ mT as estimated below.

In Fig. 1(a) we do not observe a decay with this characteristic time. On the contrary, a long-lasting signal is observed which seems to be in contradiction with the prediction. This discrepancy can be explained as follows.

The electron spin polarization is not very efficient for the experimental conditions used in the Faraday rotation experiment. The low polarization efficiency is related to a high stability of the spins of the resonantly photo-created holes which persists during their lifetime (and may go up to tens of nanoseconds for resident holes³⁴). As a result, the holes recombine predominantly with the photo-created electrons and almost no spin polarization is transferred to the resident electrons. That is why the one-nanosecond decay of the polarization cannot be resolved. Still, because this small electron spin polarization lives for a long time in the microseconds range for the QDs under study³³, a long-lasting contribution can build up during the many pump pulses within the signal recording time, so that it becomes observable and is almost constant in the scanned range of delays.

The magnitude of the spin z -projection depends on the ratio of B and B_f . It decreases with decreasing external magnetic field and falls to 1/3 of its initial value S_0 (determined by the optical excitation) at $B = 0$ corresponding to $B_t = B_f$, as it becomes randomly distributed over all directions⁴. In the other limit of strong $B \gg B_f$, B_t is mostly directed along the z -axis and the spin projection is retained up to its initial value S_0 . The theoretical magnetic field dependence of the electron spin polarization obtained by Merkulov *et al.*⁴ for a Gaussian statistics of the NSF can be approximated by the form³⁵:

$$S(B) = S_m \left(1 - \frac{A_f}{1 + (B/B_f)^2} \right), \quad (2)$$

where A_f is the amplitude of the dip and S_m is the spin

polarization at large magnetic fields. We use this function for quantitative analysis of our experimental data.

The FWHM of the dip may serve as a measure of the effective magnetic field of the NSF. As seen from the inset in Fig. 1(a), B_f is about 10 mT and 15 mT for QD samples #1 and #2, respectively³⁶. Theoretical estimates for GaAs QDs with 10^5 nuclei^{4,5} give very similar values. The fluctuation field B_f is much smaller (about 0.3 mT) for the reference (In,Ga)As/GaAs QWs. The strength of B_f depends on the electron localization volume, i.e., on the number N_L of nuclei at which the electron density has a notable magnitude: $B_f \propto 1/\sqrt{N_L}$. In quantum wells, the electron is only weakly localized by interface fluctuations along the two in-plane directions. Therefore its localization volume is large compared to the QD case and B_f is small. This is in accord with our experimental findings. From the B_f -ratio of ~ 70 for the QDs and QWs under study we conclude that the electron-localization volume in the wells is about three orders of magnitude larger than that in the dots.

The Faraday rotation technique is restricted, however, by several limitations for studying nuclear spin effects. As described, under the used low field conditions the optical pumping of the electron spin which we could achieve was quite small. Correspondingly, also the magnitude of the DNP under optical excitation with fixed helicity was quite small. Further, the FR signal does not have a natural scale and, therefore, it is unclear what degree of electron spin polarization is achieved in these experiments. Finally, the background signal related to scattered light of the pump beam prevents detection of the spin depolarization by the NSF with high accuracy.

IV. NSF AND DNP IN PL POLARIZATION

To study the effects of NSF and DNP more quantitatively, we used another experimental method, namely we exploited the effect of negative circular polarization (NCP) of the PL which appears for the studied QDs under certain experimental conditions. We excited the QDs quasi-resonantly (via intra-dot optical transitions) or to the low-energy wing of the wetting layer absorption band at energy $E_{exc} = 1.467$ eV. We found that there is no principal difference in the PL polarization for these two excitation conditions. The PL reveals circular polarization under circularly polarized excitation [see Fig. 2(a) and (b)]. The polarization degree has been calculated by: $\rho_c = (I^{++} - I^{+-})/(I^{++} + I^{+-})$, where I^{++} (I^{+-}) is the PL intensity for co- (cross-) polarization of excitation and detection. The sign of polarization for the lowest QD optical transition is negative, so that the PL intensity is stronger in cross- than in co-polarization. This is confirmed by the PL kinetics which has been measured at the energy of the PL band maximum [Fig. 2(c) and (d)]. For the further study of the NCP effect, we used excitation at an energy $E_{exc} = 1.467$ eV because excitation at lower energy requires much stronger pumping pow-

ers due to the smaller absorption of the intra-dot optical transitions.

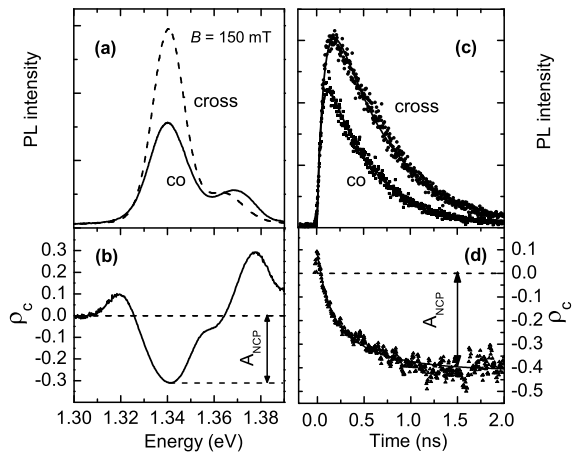


FIG. 2: (a) PL spectrum of sample #1 for co- ($\sigma^+\sigma^+$, solid curve) and cross- ($\sigma^+\sigma^-$, dashed curve) polarization of excitation and detection. Excitation at $E = 1.467$ eV with a power density $P = 20$ W/cm² for $B = 150$ mT; $T = 2$ K. (b) Spectrum of the circular polarization degree of the PL resulting from (a). (c) PL kinetics measured at $E_{PL} = 1.340$ eV at $B = 150$ mT in the two polarization configurations. (d) Polarization kinetics of the PL resulting from (c).

NCP of the ground state PL has been reported earlier for InAs^{26,37,38,39}, InP^{24,40}, and GaAs⁴¹ QDs. Although different mechanisms of NCP formation for singly negatively charged QDs have been discussed^{24,37,39,40,41}, it is commonly accepted that the large value of the NCP observed under strong optical excitation is due to accumulation of spin polarization by the resident electrons. The mechanism of the electron spin orientation is related to the spin relaxation of the photocreated holes in the QDs. These depolarized holes recombine with non-polarized resident electrons. Correspondingly, polarized electrons provided by the optical excitation are accumulated in the QDs.

The hole spin is quite stable when the hole is in the QD ground state³⁴. Therefore the efficiency of spin polarization of the resident electrons is not high for optical excitation far below the wetting layer transition. Probably this is the reason why we did not observe an NCP exceeding 20% for intra-dot excitation with an energy $E_{exc} < 1.43$ eV.

The mechanism of NCP for high-energy excitation, when free electrons and holes are created in the barrier layers, may be related to dark exciton formation⁴⁰. However, for quasi-resonant excitation when dark excitons cannot be created, the electron-hole spin flip-flop process plays the main role for NCP^{24,37,41,42}. In our subsequent analysis, we consider this process to be responsible for the NCP observed in our experiments.

The detailed NCP formation via the flip-flop process

goes as follows. If the resident electron is polarized, a photocreated electron with the same spin polarization cannot relax to the ground state because of Pauli principle unless flipping its spin. The flip is most efficient if accompanied by a simultaneous flop of the hole spin. As a result of this flip-flop process, the electron spins become paired to a singlet and the spin of the hole is inverted. Recombination of the hole with one of the electrons gives rise to emission of a σ^+ (σ^-) polarized photon for σ^- (σ^+) polarization of the excitation. This corresponds to a negative sign of polarization. The analysis also shows²⁴ that the amplitude of the NCP, A_{NCP} , extracted from the PL kinetics may be used as a measure of the spin polarization of the resident electron [see Fig. 2(d)]. In particular, for high enough spin polarization, the approximate relation

$$A_{NCP} \approx 2 \langle S_z \rangle \quad (3)$$

is valid. The factor “2” appears because the theoretical upper limit $A_{NCP} = 1$ for NCP, while for the electron spin projection onto the optical axis of excitation, $\langle S_z \rangle = 1/2$. We will use relation (3) in our subsequent analysis of the experimental data.

The amplitude of the NCP obtained in time integrated PL at the maximum of the emission band is slightly smaller than the one obtained from PL kinetics [compare Fig. 2(b) and (d)] due to averaging the polarization over the PL pulse. In this work, we studied the behavior of A_{NCP} mainly in time integrated PL because of the related simplicity of measuring the magnetic field dependence of A_{NCP} through scanning the field strength. We neglect the small difference between the A_{NCP} values obtained in time resolved and time integrated experiments and consider the time integrated value as a quantitative characteristic of the spin polarization of the resident electrons.

We measured the magnetic field dependence of A_{NCP} at different pump-power densities of optical excitation. Two regimes of circular polarization modulation of the excitation have been used. In the first one, the polarization was rapidly switched from σ^+ to σ^- . In this case, DNP did not build up which allowed us to study the NSF effect only. For DNP-studies excitation with predominate polarization σ^+ or σ^- was used. A representative set of the obtained results for sample #1 is given in Fig. 3.

A. Nuclear spin fluctuations

First we discuss the NSF effect [Fig. 3(b)]. The magnetic field dependence of the PL polarization is seen to reveal a dip around $B = 0$ which is very similar to the one observed in the Faraday rotation experiment. Therefore we treat the field dependence of the PL polarization also in the frame of the model used above for description of the FR experiments, even though the picture may be more complex under non-resonant PL excitation due to

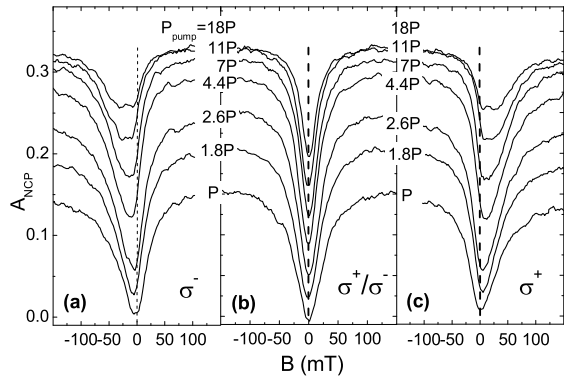


FIG. 3: Magnetic field dependence of the NCP amplitude for (a) σ^- , (b) σ^+/σ^- , and (c) σ^+ polarization of the excitation at different pump-power densities given at each curve. Sample #1. $T = 2$ K. $P = P_0 = 1$ W/cm 2 .

the energy relaxation processes. A theoretical simulation of the NSF effect in annealed InAs QDs³⁵ gives rise to a similar dip in the electron spin polarization with a FWHM which is close to the one observed at low pumping. This result further supports our interpretation of the dip.

Two important effects are seen with increasing pump power. First, the FWHM of the dip *decreases* from 30 mT at 1 W/cm 2 to 15 mT at 30 W/cm 2 . Second, the amplitude of the dip A_f normalized to the PL polarization magnitude, A_m , measured at $B \gg B_f$ also decreases with pump power [see Fig. 4(c)]. These dependencies are shown in Figs. 4(a) and (b). Both effects point out that the influence of the NSF in the electron spin depolarization becomes weaker when optical pumping becomes stronger even when no dynamic nuclear polarization appears due to modulation of the excitation polarization. We discuss these effects quantitatively in the next section.

1. “Frozen” nuclear spin fluctuations

To understand the observed behavior of the electron spin polarization, we start by considering the effect of “frozen” nuclear spin fluctuations. For this purpose, we use a simple model based on the approach developed by Merkulov *et al.*⁴ We assume that the statistics of the α -component ($\alpha = x, y,$ and z) of the NSF field can be described by a Gaussian function for the probability density distribution:

$$W(B_{f\alpha}) = \frac{1}{\sqrt{\pi}\Delta_\alpha} \exp\left[-\frac{(B_{f\alpha})^2}{\Delta_\alpha^2}\right]. \quad (4)$$

Here Δ_α is the dispersion of the $B_{f\alpha}$. We emphasize that the observation of a drop of the NSF field B_f with

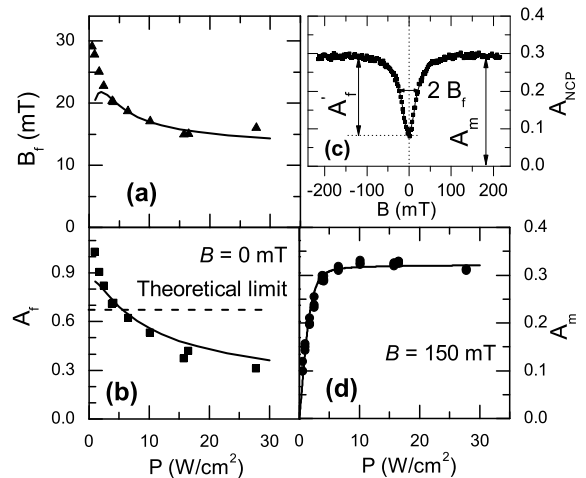


FIG. 4: Pump power dependencies of the effective magnetic field of the NSF, B_f , (a) and of the normalized amplitude of the spin polarization dip, $A_f = A'_f/A_m$, (b) for sample #1⁴³. The “theoretical limit” line shows the dip depth, $A_f = 2/3$, expected for “frozen” NSF with spatially isotropic distributions⁴. Solid lines are calculated in the frame of the “melted” NSF model using Eqs. (5,8,9) with the parameters $\Delta_z = 15$ mT, $\tau_{e0} = 3$ μ s, $\tau_{em} = 60$ μ s. Panel (c) shows a typical dip in the NCP amplitude used to explain the notations. (d) Pump power dependence of the NCP amplitude at $B = 150$ mT. The solid line is calculated using Eqs. (3,8) with the parameters $\langle S_{zf} \rangle = S_m = 0.16$ and $T_{exc}^0 = 10$ μ s.

increasing pump power in Fig. 4(a) cannot be explained by assuming that these dispersions stay isotropic under optical pumping of the nuclear spins. Therefore, in contrast to Ref. 4, we suggest that the distributions become unequal when pumping the nuclear spin system by alternately polarized electron spins: $\Delta_x = \Delta_y \neq \Delta_z$. With this assumption we have calculated the z -component of the ensemble-averaged electron spin polarization in the field of “frozen” NSF as function of the external magnetic field:

$$\langle S_{zf} \rangle = 2\pi \int_{-\infty}^{\infty} W(B_{fz}) dB_{fz} \int_0^{\infty} W(B_\rho) S_z(B) B_\rho dB_\rho. \quad (5)$$

Here we assumed a cylindrical symmetry of the nuclear spin distribution and defined the radial field $B_\rho = [B_{fx}^2 + B_{fy}^2]^{1/2}$ with a distribution $W(B_\rho) = W(B_{fx})W(B_{fy})$. $S_z(B)$ is the time-averaged z -component of the electron spin polarization reduced relative to its initial value S_m due to its fast precession about the total magnetic field, $\mathbf{B}_t = \mathbf{B}_f + \mathbf{B}$, for each particular configuration of the fluctuating nuclear field \mathbf{B}_f [see

Fig. 1(c)]:

$$S_z(B) = S_m[\cos\gamma(B)]^2 = \frac{(B_{fz} + B)^2}{(B_{fz} + B)^2 + B_\rho^2}, \quad (6)$$

where $\gamma(B)$ is the angle between \mathbf{B}_t and the initial electron spin orientation. For the averaging in Eq.(5) we used distribution functions $W(B_{f\alpha})$ with equal excitation power dependent half widths for the transverse NSF components:

$$\Delta_y = \Delta_x = \frac{\Delta_x^0}{\sqrt{1 + kP}}, \quad (7)$$

where k is a scaling factor for the excitation power P . The power dependence (7) has been determined in the model described in Appendix A.

The results of the calculations for the magnetic field dependence of the electron spin polarization at different excitation powers are shown in Fig. 5(a). The dip profile is well approximated by eq. (1) if we use the parameter $B_f = 1.39\Delta_z$ at low excitation powers when $\Delta_x = \Delta_z$. In the calculations of the power dependence, we use a value $k = 2/3 \text{ cm}^2/\text{W}$ to obtain the approximately two-fold decrease of the dip at $P = 30 \text{ W}/\text{cm}^2$, as observed experimentally [see Fig. 4(b)]. The dip FWHM and amplitude are shown in Fig. 5(c) and (d) by the dashed lines. The decrease of the dip amplitude observed at strong pumping can be satisfactorily explained by the decrease of the transverse component of the NSF.

2. “Melted” nuclear spin fluctuations

The model considered above allows us to describe the tendency in the dip behavior at relatively high excitation powers. However, for weak excitation when the process of optical spin polarization is slow, the model of “frozen” NSF cannot describe the increase of the dip amplitude up to unity [see Fig. 4(b)] as well as the small magnitude of the spin polarization even at large magnetic fields [Fig. 4(d)].

To describe this limit, we consider a slow variation of the NSF in time as discussed by Merkulov *et al.*⁴. These “melted” NSF may further depolarize the electron spin during a characteristic time in the microseconds range. Depolarization can occur only when the intrinsic electron spin lifetime (i.e., the one not related to the NSF effect) is large enough. Studies of the spin coherence in our QDs in presence of a transverse external magnetic field, when the NCP effect is suppressed, show a characteristic spin relaxation time of the resident electrons in the microseconds range^{31,33,44}.

For determining the spin polarization along the z -axis, we have solved a rate equation model for the populations of the spin-split electron states. Besides we have taken into account that the spin polarization is measured in our experiments in the second half of a long pulse from $\tau_p/2$

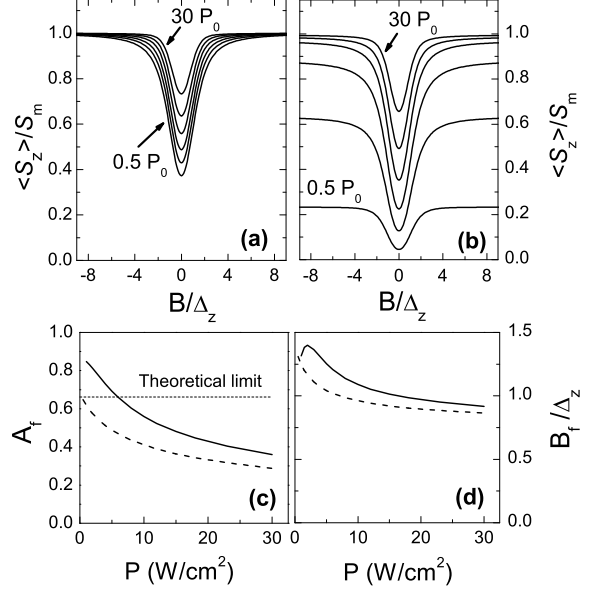


FIG. 5: (a) Magnetic field dependence of $\langle S_z \rangle$ (normalized to S_m) calculated using the model of “frozen” NSF for different excitation densities: $P = 0.5, 1.5, 3, 6, 12, 30 \text{ W}/\text{cm}^2$. (b) The same for “melted” NSF. (c) Dependence of the dip amplitude, A_f , on the power density for “melted” (solid line) and “frozen” (dashed line) NSF. (d) The same for the effective magnetic field, B_f .

to τ_p . Details are described in Appendix A. The resulting spin polarization is given by:

$$\langle S_z \rangle = \langle S_{zf} \rangle \left[\frac{2}{\gamma\tau_p} \left(\Delta n_0 + \frac{\gamma_{exc}}{\gamma} \right) \times (\exp(-\gamma\tau_p/2) - \exp(-\gamma\tau_p)) - \frac{\gamma_{exc}}{\gamma} \right], \quad (8)$$

where $\langle S_{zf} \rangle$ is the spin polarization conserved after action of the “frozen” NSF, given by Eq. (5). $\gamma = \gamma_e + \gamma_{exc}$, with the excitation rate $\gamma_{exc} = \gamma_{exc}^0 P$, where γ_{exc}^0 is the rate at $P_0 = 1 \text{ W}/\text{cm}^2$, and γ_e is the electron spin relaxation rate due to the time variations of the NSF. Δn_0 is the population difference between the two spin-split levels right before the pulse. This population difference was created by the preceding pulse with opposite circular polarization, which has partially relaxed during the dark time between pulses.

Above all, we discuss the pump power dependence of the electron spin polarization measured in an external magnetic field sufficient for suppressing the NSF effect [Fig. 4(d)]. The polarization saturates at a level of about 30% of its maximal value for excitation densities $P > 5 \text{ W}/\text{cm}^2$. This value is considerably smaller than typically observed in single dot spectroscopy¹⁵. We attribute this difference mainly to the coexistence of neutral, singly charged and multiply charged dots in the

QD ensemble³⁴. The PL of the neutral QDs is linearly polarized or unpolarized because of the anisotropic exchange interaction of electrons and holes in the QDs. The PL polarization of the multiply charged QDs is reduced too^{24,39}. The contribution of these dots reduces the total PL polarization of the ensemble, as only the singly charged dots provide a high polarization of the emission.

We use Eq. (8) to analyze the power dependence in Fig. 4(d) quantitatively. For this purpose, we use an electron spin relaxation rate, $\gamma_e = \gamma_{em} \approx 1/6 \mu\text{s}^{-1}$, as measured in Ref. 44 for this sample in presence of a magnetic field suppressing the NSF, and consider quantity γ_{exc}^0 as fitting parameter. As seen from Fig. 4(d), the fit satisfactorily reproduces the experiment. The obtained value of the fitting parameter $\gamma_{exc}^0 = 0.1 \mu\text{s}^{-1}$ means that the spin orientation of the resident electron is on average restored during a time interval $T_{exc}^0 = (\gamma_{exc}^0)^{-1} = 10 \mu\text{s}$ by optical excitation with a power density $P_0 = 1 \text{ W/cm}^2$.

This value can be compared with a simple estimate based on the experimental conditions and the structural parameters of our sample. Taking into account the total QD density in the 20 layers, $\rho_{QD} \sim 4 \times 10^{11} \text{ cm}^{-2}$ [see Ref. 31], we estimate that about 100 photons hit each dot during T_{exc}^0 at $P_0 = 1 \text{ W/cm}^2$. Further, only a small fraction, a , of these photons is absorbed at the excitation photon energy $\hbar\omega = 1.467 \text{ eV}$. Our measurements show that the probability of absorption is about 20 %. Finally, the efficiency of electron spin polarization, q , most likely is relatively small [e.g., $q = 0.05$ for InP QDs²⁴]. From these estimates it is reasonable that the product $a \cdot q$ can be as small as 0.01 and therefore only one photon out of 100 impinging photons gives rise to polarization of a resident electron spin during T_{exc}^0 .

Let us consider now the magnetic field dependence of the spin polarization at low excitation density. In absence of a magnetic field, the effective time $\tau_{e0} = (\gamma_{e0})^{-1}$ of electron spin relaxation due to interaction with the “melted” NSF is on the order of a few microseconds^{4,29}. Application of a magnetic field suppresses the effect of the “melted” NSF and, correspondingly, slows down the electron spin relaxation²⁹. At present, there is no quantitative theoretical description of the field dependence of the electron spin relaxation rate. Therefore we use a phenomenological dependence based on the experimental data by Pal *et al.*²⁹:

$$\gamma_e(B) = \gamma_{em} + \frac{\gamma_{e0}}{1 + (B/B_f)^2}. \quad (9)$$

The second term on the right hand side describes the suppression of spin transfer to the nuclear spin system when the angle between the electron spin and the total magnetic field [see Fig. 1(c)] becomes small and, correspondingly, the spin precession is inefficient. In the following calculations, γ_{e0} is considered as fitting parameter.

We use Eqs. (5,8,9) to determine the magnetic field dependence of $\langle S_z \rangle$. The results of these model calculations are shown in Figs. 5(b)-(d) by the solid lines. In Fig. 4(a) and (b), the calculated dependencies for the depth and

halfwidth of the dip are compared with the experiment. As seen, the dependences of A_f and B_f are well reproduced in the main range of pump densities except for small values $P < 3 \text{ W/cm}^2$.

So, the presented analysis allows us to explain phenomenologically the main features of the electron spin polarization in presence of the NSF. The main assumption we have used to explain the suppression of the NSF effect under strong pumping is the reduction of the transverse NSF component relative to the longitudinal one, for which the possible physical reason will be discussed by the end of the next section. Consideration of the time variations of the NSF (“melted” NSF) allowed us to explain semi-quantitatively the dip width and amplitude also in the limit of low excitation densities [see Fig. 4(a) and (b)]. There is, however, some disagreement between theory and experiment at this low excitation. One of the possible reasons is that relation (2) becomes invalid when the average spin polarization of the resident electrons is small²⁴. We also consider Eq. (9) to be oversimplified to describe correctly the electron-nuclear spin dynamics in this case. Further theoretical and experimental investigations are needed to clarify this problem.

B. Dynamic nuclear polarization

The observed considerable suppression of the NSF transverse components may hint a strong polarization of the nuclear spins under the applied experimental conditions. To check this, we have studied the DNP maintaining the experimental conditions used in the NSF study except for the modulation of the optical polarization. Usually DNP is studied for a fixed polarization of optical excitation²⁸. We, however, still used partial modulation of the polarization to avoid modifications of the optical setup. We used a relatively long pulse ($\tau_p = 22.5 \mu\text{s}$) of one polarization (σ^+ or σ^-) and a three times shorter pulse (one pulse train) of opposite polarization (σ^- or σ^+ , correspondingly) with the same peak intensity. The dark time between the pulses was $2 \mu\text{s}$ and the repetition frequency of the pulses was 25 kHz . This excitation protocol allowed us to obtain a time-averaged net polarization of one helicity and, correspondingly, to polarize the nuclei.

As seen from Fig. 3(a) and (c), such excitation results in a shift of the dip position away from zero magnetic field. This effect is shown in more detail in Fig. 6 for an excitation power density $P = 16 \text{ W/cm}^2$. The sign of the shift depends on the helicity of the light polarization and the shift increases with pump power density. Both observations are explained by DNP.

The effective magnetic field of the DNP, B_N , is directed along the external magnetic field or along the opposite direction, depending on the pump helicity, so that the total magnetic field, $B_t = B + B_N$, increases or decreases relative to the external magnetic field, B . The magnetic field dependence of the PL polarization is de-

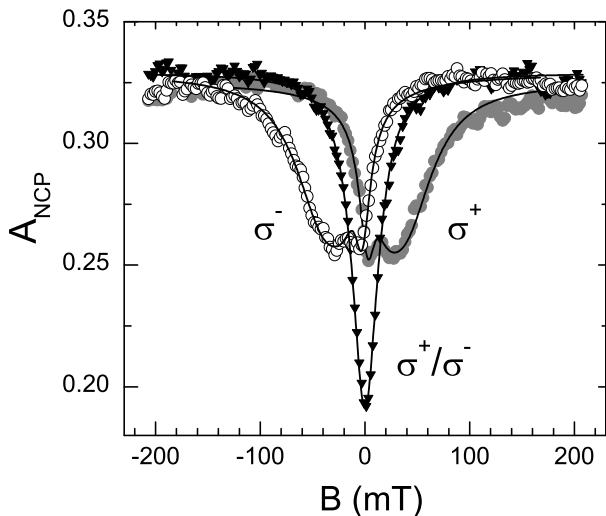


FIG. 6: Magnetic field dependence of the electron spin orientation for sample #1 under σ^- (open circles), σ^+ (filled circles) and σ^+/σ^- (triangles) polarized excitation with $P_{exc} = 16 \text{ W/cm}^2$. Lines are fits by Eqs. (10,11).

scribed by an equation similar to Eq. (2):

$$A_{NCP}(B) = A_m \left(1 - \frac{A_f}{1 + [(B + B_N)/B_f]^2} \right). \quad (10)$$

The dip in the electron spin orientation due to the NSF is still present as long as a total orientation of the nuclear spins has not been achieved, and should occur at $B_t = 0$ when $B_N = -B$. Thus the value of the dip shift may serve as a measure for the DNP effective magnetic field. The increase of the dip shift with power is inherently explained by the increase of the DNP.

Fig. 6 shows one more narrow dip in the PL polarization which appears at nearly zero magnetic field for σ^+ and σ^- polarized excitation. The origin of this dip is related to destruction of the DNP by dipole-dipole interaction between the nuclear spins when the external magnetic field becomes smaller than the local field, B_L , acting on a nuclear spin through its neighbors. This effect gives rise to the following dependence of the DNP on the magnetic field²⁸:

$$B_N(B) = \frac{B_{Nm}}{1 + [B_L/(B + B_e)]^2}, \quad (11)$$

where B_{Nm} is the maximal nuclear magnetic field reached for fixed circular excitation at $B \gg B_L$.

In Equation (11), we also took into account the effective magnetic field of the electron at a nuclear site (Knight field), B_e . We will not discuss this effect in detail⁴⁵ and consider B_L and B_e as fitting parameters. B_e determines the shift of the narrow dip away from zero magnetic field. Its value can reach several milliTesla for the strongly localized electrons in QDs¹⁴. Our fit gives $B_e \sim 10 \text{ mT}$. The parameter B_L characterizes the dip

width whose value is much larger in our case than the typical local field (fraction of milliTesla⁴⁵). We assume that the dip width increase is mainly due to the spread of the QD parameters, in particular the Knight field, in the ensemble.

Examples of fitting the PL polarization by Eqs. (10,11) are shown in Fig. 6. The fit reproduces the magnetic field dependence of A_{NCP} ⁴⁶ well which allows us to reliably determine the effective magnetic field of the DNP. Its dependence on the excitation power density is shown in Fig. 7.

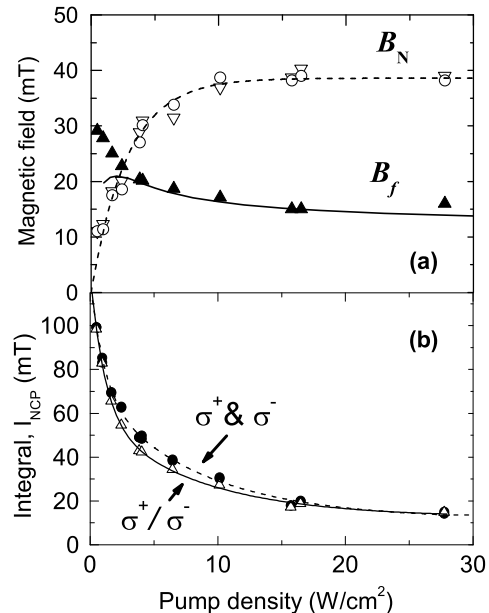


FIG. 7: (a) Effective magnetic field of the DNP, B_N , as function of pump density. Circles and triangles are the experimental data for σ^- and σ^+ polarized excitation, respectively; the dashed line is a guide to the eye. Data for the effective magnetic field of the NSF B_f from Fig. 4(a) are shown for comparison. (b) Integral of the dip as function of the pump density calculated by Eq. (12) for σ^+ - and σ^- -polarized excitation (circles), as well as for σ^+/σ^- -polarized excitation (triangles). Solid lines are guides to the eye. Data have been taken for sample #1.

B_N rapidly rises with excitation power in the same range in which the NSF field decreases and the electron spin orientation increases [compare with Fig. 4(d)]. The DNP field saturates at a value of about 40 mT at strong pumping. This value is small relative to the theoretical limit of a few Tesla when all the nuclei have been polarized²⁸.

Simultaneously the NSF value does not decrease considerably any further. To demonstrate this more clearly, we have calculated the integral of the dip area in the electron spin polarization by taking the difference between

the line $y = A_m$ and the function $y = A_{NCP}$ normalized to A_m , [see Fig 4(c)]:

$$I_{NCP} = \int (1 - A_{NCP}/A_m) dB \quad (12)$$

We consider this quantity as a measure of the effect of the fluctuating nuclear field on the electron spin polarization. As seen from Fig 7(b), the integral I_{NCP} and correspondingly the NSF decrease strongly with increasing pumping for all used excitation polarization configurations.

V. DISCUSSION

It is well established now that a significant polarization of the nuclei takes a long time of optical pumping in the seconds or minutes range^{3,28,47} and the nuclear polarization degree rises highly nonlinearly with time^{19,48}. Due to the partially modulated excitation polarization with a rather short period $T = 40 \mu s$ (see Sect. II) in our experiments, we effectively study the early stage of the nuclear polarization dynamics. Experimental studies⁴⁸ have confirmed that a B_N with a magnitude of a few tens of milliTesla is established on a sub-millisecond time scale at strong enough pumping.

A detailed theoretical analysis of the electron-nuclear spin dynamics still represents a challenging problem^{49,50}. It can be discussed qualitatively taking into account the different stages of the DNP formation which occur on very different time scales. In the early stage, the dynamics of the nuclear polarization is determined by the fast precession of the electron spin about B_f with a period in the nanoseconds range⁴. Each polarization event interrupts this precession, resulting in transfer of angular momentum between the electron and nuclear spin systems. The non-uniformity of the electron density distribution does not play an important role at this stage because it gives rise to much slower processes. E.g., it causes a slow precession of the NSF and consequently electron spin relaxation on a characteristic time scale three orders of magnitude longer than that of the electron spin relaxation in the “frozen” NSF⁴.

As we address in effect the early DNP stages, we may use in our analysis of the experimental data a simplified approach based on the “box” model as well as its generalization^{49,51,52}. The goal of our analysis is to compare qualitatively the dynamics of the nuclear spin polarization and that of the suppression of the transverse NSF components. The simple version of the box model assumes the electron density to be uniformly distributed over the QD volume^{49,51,52}. It gives B_N -fields whose strengths are comparable to the fluctuating nuclear field B_f only. Our experimental results agree well with this result: $B_f = 30$ mT (at weak excitation keeping the nuclear system non-polarized) and $B_N = 40$ mT, see Fig. 7(a). The simple box model also predicts that, in spite of the small achievable nuclear spin polarization, the transverse

component of B_f may be considerably decreased by optical pumping, also in agreement with our results.

To understand the underlying physics, we have performed model calculations using the simple and extended box models. Details of these models are given in Appendix B. The effective magnetic fields of the DNP and NSF destroying the electron spin polarization are given by the equations^{28,35}:

$$\begin{aligned} B_N &= \frac{A_{hf}}{g_e \mu_B} \langle \hat{I}_z \rangle, \\ B_f &= \frac{A_{hf}}{g_e \mu_B} \sqrt{2 \langle \hat{I}_x^2 + \hat{I}_y^2 \rangle}. \end{aligned} \quad (13)$$

Here A_{hf} is the constant of the hyperfine electron-nuclear spin interaction and $\langle \hat{I}_\alpha \rangle$ ($\alpha = x, y, z$) is the averaged value of the α -component of the total nuclear spin.

When the nuclei are non-polarized, $\langle \hat{I}_z \rangle = 0$ and $\langle \hat{I}_x^2 + \hat{I}_y^2 \rangle = 2/3 \langle \hat{I}^2 \rangle$. Assuming $I_i = 1/2$ (in units of \hbar) for all nuclear spins, $\langle \hat{I}^2 \rangle = (3/2)N$ where $2N$ is the number of nuclei interacting with the electron. From these relations follows $(B_f)_{non} = A_{hf}/(g_e \mu_B) \sqrt{2N}$ for the non-polarized nuclei.

From the box model calculations we can derive the strongly polarized state of the nuclear spin system achievable under strong (but short) optical pumping. The average value of \hat{I}_z for this state is given by:

$$\langle \hat{I}_z \rangle \approx 2\sqrt{\frac{N}{\pi}}. \quad (14)$$

The average polarization of the nuclear spin system remains small. Therefore the effective magnetic field of the DNP is also small: $B_N \approx A_{hf}/(g_e \mu_B) 2\sqrt{N/\pi}$, which is about the effective field of the NSF for a non-polarized nuclear system. At the same time, the transverse component of the NSF tends to be considerably reduced in the strongly polarized state:

$$\langle \hat{I}_x^2 \rangle + \langle \hat{I}_y^2 \rangle = \langle \hat{I}_z \rangle. \quad (15)$$

From this result it follows that the transverse component of the NSF is reduced to: $(B_f)_{pol} = A/(g_e \mu_B) 2\sqrt{N/\pi}$, which is small compared to the initial value $(B_f)_{non}$. For instance, $(B_f)_{pol}/(B_f)_{non} \approx 0.07$ for $2N = 10^5$ nuclei.

The assumption about homogeneity of the electron density used in the box model is not valid in real QDs. Due to the inhomogeneity of the density, nuclear spin sub-systems with different I interact with each other (via hyperfine interaction with the electron) which results in a larger achievable spin polarization than the one predicted by the box model. In Ref. 52, an extended model in which the electron density is approximated by a series of step functions (“graded box” model) is considered. The upper limit of the nuclear spin polarization predicted by this model is: $\langle \hat{I}_z \rangle \propto \sqrt{kN}$ where k is the number

of steps in the function. The graded box model also predicts that $(B_f)_{pol} / (B_f)_{non} \propto \sqrt[4]{k/N}$. A limited number of steps $k \ll N$ should give an appropriate description of the electron wavefunction/density distribution in the studied annealed QDs. Still this extended model predicts a nuclear spin polarization, which is only several times larger than the one predicted by the simple box model. Similar to the simple box model, it also predicts a strong suppression of the NSF. These results support the main conclusions derived from the simple box model. Another verification of the box model has been done by Zhang et al.⁵³ using numerical simulations for a limited number of nuclei.

From these conclusions, we may consider the following scenario of the nuclear spin dynamics. The optical pumping rapidly polarizes the nuclei within sub-systems each with a fixed I , thus creating relatively small DNP and, at the same time, strongly suppressing the transverse components of the NSF. Further pumping gives rise to a slow increase of the DNP. In our experiments, however, this long-term buildup is prevented by the partially modulated polarization of the pumping. We also note that the strong suppression of the NSF effect favors formation of an electron-nuclear spin polaron as reported in Ref. 26.

Dynamic nuclear polarization is usually treated in terms of lowering the nuclear spin temperature²⁸. The small effective magnetic field B_N which we observed for σ^+ - and σ^- -polarized excitation means that the decrease of the nuclear spin temperature is small for our experimental conditions. At the same time, the considerable suppression of the NSF effect for the same conditions indicates a strong modification of the nuclear spin dynamics. We emphasize that an equally efficient suppression of the NSF effect is observed for the σ^+/σ^- excitation protocol [see Fig. 7(b)] when no spin temperature decrease is expected. Therefore we conclude that the concept of an effective temperature cannot adequately describe the spin state of the nuclear system in our case and we should describe it in the frame of a decrease of the entropy of the system. We believe that this problem deserves further theoretical investigations.

VI. CONCLUSION

The experiments performed here have allowed us to determine the effective magnetic field of the nuclear spin fluctuations in an ensemble of (In,Ga)As quantum dots. This NSF field is about 30 mT at weak excitation and considerably decreases with pumping. We explain this effect by a decrease of the transverse component of the nuclear spin fluctuations under optical excitation with modulated polarization helicity.

We also considered the time variations of the nuclear spin fluctuations to explain the electron spin polarization at weak excitation. These variations can partly explain the increase of the electron polarization dip width and depth with decreasing pumping although further inves-

tigations are required for a quantitative modeling of the experiment.

We compared the NSF field with that of the DNP appearing for very similar experimental conditions. The effective magnetic field of the polarization observed under strong excitation for a rather short time is about 40 mT which is by orders of magnitude smaller than the theoretically predicted upper equilibrium limit.

Both the strong suppression of the NSF and the small DNP are satisfactorily explained in the framework of the box model for the electron-nuclei hyperfine interaction. The optical pumping rapidly polarizes the nuclei within sub-systems consisting of nuclear states with fixed total angular momentum. This process results in a strong suppression of the transverse components of the NSF and in a relatively small average polarization of the nuclear spins. Further nuclear polarization is a much slower process which has not been realized for the experimental conditions in the present studies.

ACKNOWLEDGMENTS

The authors thank I. Ya. Gerlovin for fruitful discussions. The work was supported by the Deutsche Forschungsgemeinschaft (GK726 and Grants Nos. BA1549/11-1 and 436 RUS 17/144/05) and the BMBF research program “nanoquit”. The work was partly supported by ISTC (grant 2679), by the Russian Ministry of Science and Education (grant RNP.2.1.1.362) and by the Russian Foundation for Basic Research. R. Oulton thanks the Alexander von Humboldt foundation for support.

APPENDIX A: CALCULATION OF ELECTRON SPIN POLARIZATION FOR FROZEN AND MELTED NSF

1. Frozen NSF

Equations (5,6) allow us to calculate $\langle S_{zf}(B) \rangle$ as function of Δ_x and Δ_z . We keep Δ_z fixed for simplicity and assume that the optical excitation gives rise to reducing the distribution parameter Δ_x . To connect its value with the power density of the optical excitation, we consider an effective number of nuclear spins, N_x , with non-zero x -projection: $N_x = I_x N_L$, where $I_x = [\langle \hat{I}_x^2 \rangle]^{1/2}$ is the averaged x -projection of a nuclear spin defined in a standard way via the spin operator \hat{I}_x squared. N_x determines the distribution parameter according to: $\Delta_x \propto \sqrt{N_x}$. The rate equation for N_x has the form:

$$\frac{dN_x}{dt} = -\gamma_{exc} N_x + \gamma_N (N_x^0 - N_x) \quad (\text{A1})$$

Here γ_{exc} is the excitation rate which is proportional to the pump power P , and γ_N is the relaxation rate of the

nuclear spin polarization. N_x^0 is the N_x in absence of excitation. From this equation we derive the power dependence of Δ_x :

$$\Delta_x = \frac{\Delta_x^0}{\sqrt{1 + \gamma_{exc}/\gamma_N}}. \quad (\text{A2})$$

Δ_x^0 ($\propto \sqrt{N_x^0}$) is the initial value of Δ_x which equals to Δ_z in the frame of our model. We then exploit that $\gamma_{exc} \propto P$, make the substitution $\gamma_{exc}/\gamma_N = kP$ in Eq. (A2), and use the parameter k to fit the calculations to the experiment.

2. Melted NSF

Let us consider the population dynamics of the spin-split electron states under excitation by a long circularly polarized pulse:

$$\begin{aligned} \frac{dn^+}{dt} &= -\gamma_{exc}n^+ - \frac{\gamma_e}{2}(n^+ - n^-), \\ \frac{dn^-}{dt} &= \gamma_{exc}n^+ + \frac{\gamma_e}{2}(n^+ - n^-). \end{aligned} \quad (\text{A3})$$

Here n^+ and n^- are the populations of the $|+\frac{1}{2}\rangle$ and $|-\frac{1}{2}\rangle$ spin states of the resident electron, respectively. The total population is normalized: $n^+ + n^- = 1$. The excitation rate $\gamma_{exc} = \gamma_{exc}^0 P$, where P is the power density of excitation and γ_{exc}^0 is the excitation rate at $P_0 = 1$ W/cm². Equations (A3) are written for the case when a circularly (say σ^+) polarized light pulse depopulates the $|+\frac{1}{2}\rangle$ state and populates the state $|-\frac{1}{2}\rangle$. γ_e denotes the spin relaxation rate due to time variations of the NSF, which tends to decrease the population difference $\Delta n = n^+ - n^-$. Solution of Eqs. (A3) leads to the following time dependence of Δn during excitation:

$$\Delta n(t) = \left(\Delta n_0 + \frac{\gamma_{exc}}{\gamma} \right) \exp(-\gamma t) - \frac{\gamma_{exc}}{\gamma}, \quad (\text{A4})$$

where $\gamma = \gamma_e + \gamma_{exc}$. Δn_0 is the initial population difference, which was created by the previous long pulse with opposite circular polarization and has partially relaxed during the dark time between the pulses. To determine Δn_0 , we take into account the duration of each long pulse, $\tau_p = 15$ μ s, and of the dark time, $\tau_d = 3$ μ s, and also the fact that Δn_0 periodically changes its sign while having the same absolute value after σ^+ and σ^- polarized pulses. Simple calculations give the expression:

$$\Delta n_0 = \frac{\gamma_{exc}}{\gamma} \left(\frac{1 - \exp(-\gamma\tau_p)}{\exp(\gamma\tau_d) + \exp(-\gamma\tau_p)} \right). \quad (\text{A5})$$

We measured the spin polarization during the second half of a long pulse from $\tau_p/2$ to τ_p . Therefore, we have to integrate Eq. (A4) over this time interval. Finally, using $S_z \propto \Delta n$, we obtain expression (8) for the spin polarization.

APPENDIX B: DESCRIPTION OF THE SIMPLE AND GRADED BOX MODELS

The box model has been described in detail in Ref. 49. It assumes that the electron-nuclear spin system is comprised of an electron spin $S = 1/2$ coupled to an even number $M = 2N$ of identical nuclei, each with spin $I_j = 1/2$ ($j = 1 \dots M$). The homogeneous distribution of the electron density over the nuclei results in an identical interaction of each nucleus with the electron. This high symmetry of the system gives rise to a Hamiltonian which depends on the *total* angular momentum of the nuclear spins: $\hat{\mathbf{I}} = \sum_{j=1}^M \hat{\mathbf{I}}_j$ (in units of \hbar). The Hamiltonian has the form:

$$\hat{H} = A_{hf} \hat{S}_z \hat{I}_z + \frac{A_{hf}}{2} (\hat{S}_+ \hat{I}_- + \hat{S}_- \hat{I}_+). \quad (\text{B1})$$

Here the standard notations for the z -projections and rising and lowering operators of the electron and nuclear spins are used. The parameter A_{hf} is the constant of the hyperfine interaction which does not depend on the nucleus number.

Due to the simple form of the Hamiltonian, it commutes with \hat{I}^2 . This gives rise to an *angular momentum conservation law* which is a specific property of the box model. The density matrix of the nuclear spin system consists of blocks corresponding to states with fixed total nuclear angular momentum I . These blocks are mutually independent, i.e., the hyperfine interaction of the nuclear spin system with a polarized electron spin may transfer the system from one state to another within the same block only, rather than between different blocks⁴⁹. In other words, the total nuclear spin system is divided into multiple non-interacting sub-systems with different momenta I .

Due to the conservation law, the average value, $\langle \hat{I}^2 \rangle$, is not changed under optical pumping and equals to that for the totally non-polarized nuclear spin system described by the high-temperature density matrix. The latter can be easily calculated using equations derived in Ref. 49:

$$\langle \hat{I}^2 \rangle = \sum_{I=0}^N W_I I(I+1). \quad (\text{B2})$$

Here W_I is the probability to obtain the eigenvalue $I(I+1)$:

$$W_I = 2^{-2N} (2I+1) \Gamma_N(I). \quad (\text{B3})$$

The factor 2^{-2N} describes the equal probability of all states, $(2I+1)$ is the number of eigenstates in a block with total angular momentum I , and $\Gamma_N(I)$ is the number of these blocks. The distribution function $\Gamma_N(I)$ has the asymptotic expression^{49,53}:

$$\Gamma_N(I) = -\frac{2^{2N}}{\sqrt{\pi N}} \frac{d}{dI} \exp\left(-\frac{I^2}{N}\right) \quad (\text{B4})$$

Equations (B2,B3,B4) give rise to the simple result:

$$\langle \hat{I}^2 \rangle = \frac{3}{2}N \quad (\text{B5})$$

which is valid for all polarization states of the nuclear spin system.

When the nuclei are non-polarized, $\langle \hat{I}_z \rangle = 0$ and non-zero value of $\langle \hat{I}^2 \rangle$ in Eq. (B5) is due to the NSF so that $\langle \hat{I}_\alpha^2 \rangle = N/2$ for $\alpha = x, y, z$.

Let us consider the strongly polarized state of the nuclear spin system achievable in the frame of the box model. Strongly polarized state means that only one state is populated in each block. Correspondingly, the density matrix has the form:

$$U_{LI} = \begin{cases} 0 & \text{when } L \neq I, \\ 2^{-2N}(2I+1) & \text{when } L = I. \end{cases} \quad (\text{B6})$$

Here L is the z -projection of the total nuclear angular momentum I . The average value of \hat{I}_z is given by:

$$\langle \hat{I}_z \rangle = \sum_{I=0}^N \Gamma_N(I) \sum_{L=-I}^I U_{LI} L \approx 2\sqrt{\frac{N}{\pi}}. \quad (\text{B7})$$

The approximate value of $\langle \hat{I}_z \rangle$ has been obtained using

the asymptotic expression (B4). Further, for each block with a given I , we obtain for the averaged square of the transverse nuclear moment:

$$\langle \hat{I}_x^2 \rangle + \langle \hat{I}_y^2 \rangle = \langle \hat{I}^2 \rangle - \langle \hat{I}_z^2 \rangle = I(I+1) - I^2 = I = \langle \hat{I}_z \rangle. \quad (\text{B8})$$

This relation is also valid for the total nuclear spin and has been already used in the main text [see Eqn. (15)].

The extended box model consider an electron density distribution in the QD, which consists of a series of step functions⁵². It is intuitive that such model can approximate the real density distribution well for an appropriate choice of the number k of steps and their widths in real space. Here we consider for simplicity equidistant steps. The electron-nuclei hyperfine interaction within one step is characterized by a constant, $A_{hf,i}$, where $i = 1 \dots k$ and all the nuclei are assumed to have the same spin.

The analysis shows⁵² that the extended box model gives a larger achievable nuclear spin polarization, $\langle \hat{I}_z \rangle \propto \sqrt{kN}$. For analysis of the NSF in the strongly polarized nuclear spin system, Eq. (15) can be used which remains valid in the frame of the extended box model. This fact has been used in the main text to come to a strong suppression of the NSF.

* Electronic address: ivan.ignatiev@mail.ru

† Present address: Department of Physics and Astronomy University of Sheffield, Hicks Building, Hounsfield Rd, S3 7RH Sheffield, UK

¹ S. W. Brown, T. A. Kennedy, D. Gammon, and E. S. Snow, Phys. Rev. B **54**, R17339 (1996).

² D. Gammon, S. W. Brown, E. S. Snow, T. A. Kennedy, D. S. Katzer, and D. Park, Science **277**, 85 (1997).

³ D. Gammon, Al. L. Efros, T. A. Kennedy, M. Rosen, D. S. Katzer, D. Park, S. W. Brown, V. L. Korenev, and I. A. Merkulov, Phys. Rev. Lett. **86**, 5176 (2001).

⁴ I. A. Merkulov, Al. L. Efros, and M. Rosen, Phys. Rev. B **65**, 205309 (2002).

⁵ A. V. Khaetskii, D. Loss, and L. Glazman, Phys. Rev. Lett. **88**, 186802 (2002).

⁶ A. V. Khaetskii and Yu. V. Nazarov, Phys. Rev. B **61**, 12639 (2000).

⁷ P.-F. Braun, X. Marie, L. Lombez, B. Urbaszek, T. Amand, P. Renucci, V. K. Kalevich, K. V. Kavokin, O. Krebs, P. Voisin, and Y. Masumoto, Phys. Rev. Lett. **94**, 116601 (2005).

⁸ L. Lombez, P.-F. Braun, X. Marie, P. Renucci, B. Urbaszek, T. Amand, O. Krebs, and P. Voisin, Phys. Rev. B **75**, 195314, (2007).

⁹ R. I. Dzhioev, V. L. Korenev, I. A. Merkulov, B. P. Zakharchenya, D. Gammon, Al. L. Efros, and D. S. Katzer, Phys. Rev. Lett. **88**, 256801 (2002).

¹⁰ R. I. Dzhioev, K. V. Kavokin, V. L. Korenev,

M. V. Lazarev, B. Ya. Meltser, M. N. Stepanova, B. P. Zakharchenya, D. Gammon, and D. S. Katzer, Phys. Rev. B **66**, 245204 (2002).

¹¹ I. Ya. Gerlovin, Yu. P. Efimov, Yu. K. Dolgikh, S. A. Eliseev, V. V. Ovsyankin, V. V. Petrov, R. V. Cherbunin, I. V. Ignatiev, I. A. Yugova, L. V. Fokina, A. Greilich, D. R. Yakovlev, and M. Bayer, Phys. Rev. B **75**, 115330 (2007).

¹² A. S. Bracker, E. A. Stinaff, D. Gammon, M. E. Ware, J. G. Tischler, A. Shabaev, Al. L. Efros, D. Park, D. Gershoni, V. L. Korenev, and I. A. Merkulov, Phys. Rev. Lett. **94**, 047402 (2005).

¹³ T. Yokoi, S. Adachi, H. Sasakura, S. Muto, H. Z. Song, T. Usuki, and S. Hirose, Phys. Rev. B **71**, 041307(R) (2005).

¹⁴ C. W. Lai, P. Maletinsky, A. Badolato, and A. Imamoglu, Phys. Rev. Lett. **96**, 167403 (2006).

¹⁵ B. Eble, O. Krebs, A. Lemaître, K. Kowalik, A. Kudelski, P. Voisin, B. Urbaszek, X. Marie, and T. Amand, Phys. Rev. B **74**, 081306(R) (2006).

¹⁶ P.-F. Braun, B. Urbaszek, T. Amand, X. Marie, O. Krebs, B. Eble, A. Lemaître, and P. Voisin, Phys. Rev. B **74**, 245306 (2006).

¹⁷ P. Maletinsky, C. W. Lai, A. Badolato, and A. Imamoglu, Phys. Rev. B **75**, 035409 (2007).

¹⁸ A. I. Tartakovskii, T. Wright, A. Russell, V. I. Falko, A. B. Vankov, J. Skiba-Szymanska, I. Drouzas, R. S. Kolodka, M. S. Skolnick, P. W. Fry, A. Tahraoui,

- H.-Y. Liu, and M. Hopkinson, Phys. Rev. Lett. **98**, 026806 (2007).
- ¹⁹ P. Maletinsky, A. Badolato, and A. Imamoglu, Phys. Rev. Lett. **99**, 056804 (2007).
- ²⁰ B. Urbaszek, P.-F. Braun, T. Amand, O. Krebs, T. Belhadj, A. Lemaître, P. Voisin, and X. Marie, Phys. Rev. B **76**, 201301(R)(2007).
- ²¹ C. Deng, and X. Hu, Phys. Rev. B **73**, 241303(R) (2006).
- ²² J. M. Elzerman, R. Hanson, L. H. Willems van Beveren, B. Witkamp, L. M. K. Vandersypen, and L. P. Kouwenhoven, Nature (London) **430**, 431 (2004).
- ²³ M. Kroutvar, Y. Ducommun, D. Heiss, M. Bichler, D. Schuh, G. Abstreiter, and J. J. Finley, Nature (London) **432**, 81 (2004).
- ²⁴ M. Ikezawa, B. Pal, Y. Masumoto, I. V. Ignatiev, S. Yu. Verbin, and I. Ya. Gerlovin, Phys. Rev. B **72**, 153302 (2005).
- ²⁵ B. Pal, M. Ikezawa, Y. Masumoto and I. Ignatiev, J. Phys. Soc. Japan **75**, 054702 (2006).
- ²⁶ R. Oulton, A. Greilich, S. Yu. Verbin, R. V. Cherbunin, T. Auer, D. R. Yakovlev, M. Bayer, I. A. Merkulov, V. Stavarache, D. Reuter, and A. D. Wieck, Phys. Rev. Lett. **98**, 107401 (2007).
- ²⁷ A. Greilich, A. Shabaev, D.R. Yakovlev, Al.L. Efros, I.A. Yugova, D. Reuter, A.D. Wieck and M. Bayer, Science **317**, 1896 (2007).
- ²⁸ *Optical Orientation*. Edited by F. Meier and B. P. Zakharchenya (North Holland, Amsterdam, 1984).
- ²⁹ B. Pal, S. Yu. Verbin, I. V. Ignatiev, M. Ikezawa, and Y. Masumoto, Phys. Rev. B **75**, 125322 (2007).
- ³⁰ W. Langbein, P. Borri, U. Woggon, V. Stavarache, D. Reuter, and A. D. Wieck, Phys. Rev. B **69**, 161301(R) (2004).
- ³¹ A. Greilich, R. Oulton, E. A. Zhukov, I. A. Yugova, D. R. Yakovlev, M. Bayer, A. Shabaev, Al. L. Efros, I. A. Merkulov, V. Stavarache, D. Reuter, and A. Wieck, Phys. Rev. Lett. **96**, 227401 (2006).
- ³² *Semiconductor Spintronics and Quantum Computation*. Edited by D. D. Awschalom, D. Loss, and N. Samarth (Springer, Berlin, 2002).
- ³³ A. Greilich, D. R. Yakovlev, A. Shabaev, Al. L. Efros, I. A. Yugova, R. Oulton, V. Stavarache, D. Reuter, A. Wieck, and M. Bayer, Science **313**, 341 (2006).
- ³⁴ S. Laurent, B. Eble, O. Krebs, A. Lemaître, B. Urbaszek, X. Marie, T. Amand, and P. Voisin, Phys. Rev. Lett. **94**, 147401 (2005).
- ³⁵ M. Yu. Petrov, I. V. Ignatiev, S. V. Poltavtsev, A. Greilich, D. R. Yakovlev, and M. Bayer, Phys. Rev. B (*submitted*); also available at arXiv:0710.5091v4.
- ³⁶ The difference in FWHM for the two QD samples is related to different localization volume of electrons^{4,35} as well as to different excitation efficiencies of the samples. Dependence of the FWHM on excitation is discussed in Sect. IV.
- ³⁷ S. Cortez, O. Krebs, S. Laurent, M. Senes, X. Marie, P. Voisin, R. Ferreira, G. Bastard, J.-M. Gérard, and T. Amand, Phys. Rev. Lett. **89**, 207401 (2002).
- ³⁸ S. Laurent, O. Krebs, S. Cortez, M. Senes, X. Marie, T. Amand, P. Voisin, and J.-M. Gérard, Physica E **20**, 404 (2004).
- ³⁹ S. Laurent, M. Senes, O. Krebs, V. K. Kalevich, B. Urbaszek, X. Marie, T. Amand, and P. Voisin, Phys. Rev. B **73**, 235302 (2006).
- ⁴⁰ R. I. Dzhiyev, B. P. Zakharchenya, V. L. Korenev, P. E. Pak, D. A. Vinokurov, O. V. Kovalenkov, and I. S. Trasov, Phys. Sol. State **40**, 1587 (1998).
- ⁴¹ M. E. Ware, E. A. Stinaff, D. Gammon, M. F. Doty, A. S. Bracker, D. Gershoni, V. L. Korenev, S. C. Badescu, Y. Lyanda-Geller, and T. L. Reinecke, Phys. Rev. Lett. **95**, 177403 (2005).
- ⁴² K. V. Kavokin, Phys. Status Solidi A **195**, 592 (2003).
- ⁴³ As seen from Fig. 4(b), the amplitude $A_f > 1$ at weak excitation which seems to contradict the relation 3. However we cannot use this relation in the low excitation limit. $A_f > 1$ indicates that the PL polarization in the time integrated measurements becomes *positive* at weak excitation. The physical origin of this positive polarization can be understood from an analysis of the PL kinetics. The PL polarization is positive right after the excitation [see Fig. 2(c) and (d)] and then approaches a negative value whose magnitude is small (a few percent) at weak excitation. Because the PL intensity is much larger in the initial time interval when the polarization is positive, the time integrated PL polarization becomes positive too.
- ⁴⁴ R. V. Cherbunin, I. V. Ignatiev, D. R. Yakovlev, and M. Bayer, Proceedings of the 15th Int. Symp. Nanostructures: Physics and Technology (NANO2007), Novosibirsk, Russia, June 25-29, 2007, p. 271.
- ⁴⁵ The Knight field for these QDs has been studied by R. Oulton, S. Yu Verbin, T. Auer, R. V. Cherbunin, A. Greilich, D. R. Yakovlev, M. Bayer, D. Reuter and A. Wieck, Phys. Status Solidi B **243**, 3922 (2006).
- ⁴⁶ We should note here that the good correspondence of the fit curves and the experimental data in Fig. 7 is related to the special timing protocol of the excitation we used. Under strong excitation with a fixed helicity of light the experimental curve shows a slower rise of A_{NCP} with increasing $|B|$ which cannot be approximated by Eqs. (10,11). We tentatively attribute this behavior to the large spread of nuclear magnetic fields in the QD ensemble which slowly develops with time. Our discussion of this phenomenon will be presented elsewhere.
- ⁴⁷ M. N. Makhonin, A. I. Tartakovskii, A. Vankov, I. Drouzas, T. Wright, J. Skiba-Szymanska, A. Russell, V. I. Falko, M. S. Skolnick, H.-Y. Liu, and M. Hopkinson, Phys. Rev. B **77**, 125307 (2008).
- ⁴⁸ S. Yu. Verbin, R. V. Cherbunin, I. V. Ignatiev, T. Auer, D. R. Yakovlev, M. Bayer, D. Reuter, A. D. Wieck, ICPS29 (*unpublished*).
- ⁴⁹ G. G. Kozlov, JETP **105**, 803 (2007).
- ⁵⁰ H. Christ, J. I. Cirac, and G. Giedke, Phys. Rev. B **75**, 155324 (2007).
- ⁵¹ S. M. Ryabchenko and Yu. G. Semenov, Zh. Eksp. Teor. Fiz. **84**, 1419 (1983) [Sov. Phys. JETP **57**, 1301 (1983)].
- ⁵² G. G. Kozlov, available at arXiv:0801.1391v1.
- ⁵³ W. Zhang, V. V. Dobrovitski, K. A. Al-Hassanieh, E. Dagotto, and B. N. Harmon, Phys. Rev. B **74**, 205313 (2006).